JCTC Journal of Chemical Theory and Computation

pubs.acs.org/JCTC Article

Development of a Force Field for the Simulation of Single-Chain Proteins and Protein−Protein Complexes

Stefano Piana,*[,§] Paul Robustelli,[§] Dazhi Tan, Songela Chen, and David E. Shaw*

Cite This: *J. Chem. Theory Comput.* 2020, 16, 2494−2507 Read Online

ACCESS | Metrics & More | Article Recommendations | Supporting Information

ABSTRACT: The accuracy of atomistic physics-based force fields for the simulation of biological macromolecules has typically been benchmarked experimentally using biophysical data from simple, often single-chain systems. In the case of proteins, the careful refinement of force field parameters associated with torsion-angle potentials and the use of improved water models have enabled a great deal of progress toward the highly accurate simulation of such monomeric systems in both folded and, more recently, disordered states. In living organisms, however, proteins constantly interact with other macromolecules, such as proteins and nucleic acids, and these interactions are often essential for proper biological function. Here, we show that state-of-the-art force fields tuned to provide an accurate description of both ordered and disordered proteins can be limited in their ability to accurately describe protein−protein complexes. This observation prompted us to perform an extensive reparameterization of one variant of the Amber protein force field. Our objective involved refitting not only the parameters associated with torsion-angle potentials but also the parameters used to model nonbonded interactions, the specification of which is expected to be central to the accurate description of multicomponent systems. The resulting force field, which we call *DES-Amber*, allows for more accurate simulations of protein−protein complexes, while still providing a state-of-the-art description of both ordered and disordered single-chain proteins. Despite the improvements, calculated protein−protein association free energies still appear to deviate substantially from experiment, a result suggesting that more fundamental changes to the force field, such as the explicit treatment of polarization effects, may simultaneously further improve the modeling of single-chain proteins and protein−protein complexes.

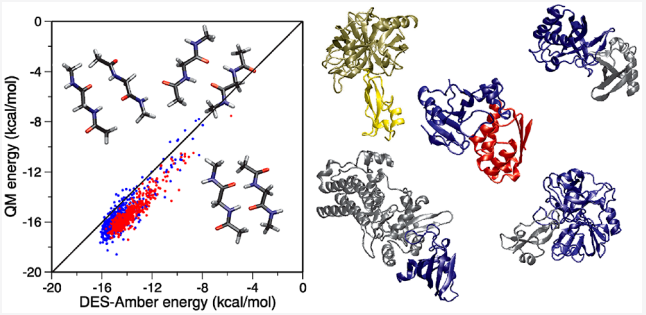

INTRODUCTION

Significant advances in technology and algorithms have in recent years been expanding the reach of molecular dynamics (MD) simulations to encompass the characteristic time scales of a progressively widening range of important biological processes. In such cases, the predictive power of simulation is often limited by the accuracy of the energy functions ("force fields") used to approximate inter- and intramolecular interactions. The accuracy of force fields in describing the structure and dynamics of proteins has traditionally been measured by comparing simulation results for relatively simple systems—small proteins or isolated protein domains—to high-quality biophysical experimental data.[1−8] These simple benchmark systems are attractive for two key reasons: simulations are relatively straightforward to set up and analyze, and large quantities of high-quality experimental data are available for comparison.

Studies of these benchmark systems have indicated that although simulations can recapitulate the structural dynamics of folded proteins with a relatively high degree of accuracy, until recently simulations of disordered proteins often showed large discrepancies when compared to experimental data, as the simulated structural ensembles were often too compact with respect to the experimental estimates.[1,2,9] This shortcoming has been greatly alleviated in recent years by applying relatively targeted changes to force fields, including the optimization of torsion parameters and the development of models with improved descriptions of solvent interactions.[1,5,9−11] In simulations of single-protein chains, the resulting state-of-the-art force fields produce more expanded structural ensembles, achieving for disordered proteins a level of accuracy comparable to that for folded proteins.[1,5,10] In living organisms, however, proteins seldom perform their functions in isolation; on the contrary, they constantly interact with other biological macromolecules such as proteins and nucleic acids. It has been unclear whether a force field that is well suited for simulations of isolated proteins would be similarly accurate in simulations of more complex, multi-

Received: October 7, 2019
Published: January 8, 2020

https://dx.doi.org/10.1021/acs.jctc.9b00251
J. Chem. Theory Comput. 2020, 16, 2494−2507

Table 1. List of Protein−Protein Complexes Used as a Benchmark for Protein Force Fields[a]

name	PDB entry	ΔG_{bind} (kcal mol^{-1} M^{-1})	ΔG_{bind} (a99SB-*disp*)		ΔG_{bind} (DES-Amber)		interface area (Å^2)
Ubq/UEV	1S1Q[82]	−4.3[83]	−8.0(4)	−7.1(3)	−8.5(3)	−7.9(5)	650
insulin dimer	1TRZ[84]	−5.5[85]	-	-	-	-	800
Ubq/Ubq-ligase	2OOB[86]	−5.8[86]	*−3.6*	*−5.4*	−6.7(1)	−6.5(2)	450
TβR-1/FKBP12	1B6C[87]	−7.6	−19.0(5)	28.4	−16(3)	−10(2)	920
Pex5p/SCP2	2C0L[88]	−9.8[88]	0(1)	4(2)	−7.9(5)	−4.4(7)	870
BPTI/MT-SP1	1EAW[89]	−12[82]	−12(1)	*1.9*	*9.8*	*1.3*	960
SGPB/OMTKY3	3SGB[90]	−12.5[90]	−3.6(6)	0.0(3)	−7.2(4)	−4(3)	660
barnase/barstar	1BRS[91]	−18[91]	2.3(2)	4.1(1)	−16.1(7)	−6.9(3)	840
BPTI/trypsin	2PTC[92]	−18[93]	−3(8)	*−15.7*	−40(20)	*1.0*	720
colE7/Im7	7CEI[94]	−19.8[95]	−10.2(7)	−7(1)	−13.0(2)	−6.8(5)	690
FAB/factor VIII	1IQD[96]	−14.1[97]	-	-	−11.7(5)	-	1020
Ad12/CAR D1	1KAC[98]	−8.9[99]	-	-	−1.7(3)	-	760
ImGP synthase	1GPW[100]	−7.9[101]	-	-	−6.4(3)	-	1070
CD2/CD58	1QA9[102]	−7.2[102]	-	-	−7.9(1)	-	690

[a]The name of the complex, the PDB entry of the experimental structure, the association free energy determined experimentally, and the values calculated for the a99SB-*disp* and DES-Amber force fields using two different sets of restraints are shown. Values in italics represent simulations in which the native complex was not reached, and the values should be considered highly unreliable. We could not compute association free energies for the insulin dimer, as it folds upon binding. For the last four complexes, only one set of simulations was run. The interface area was calculated as half of the difference between the dimer and the monomers' surface areas accessible to a probe with a 1.5-Å radius.

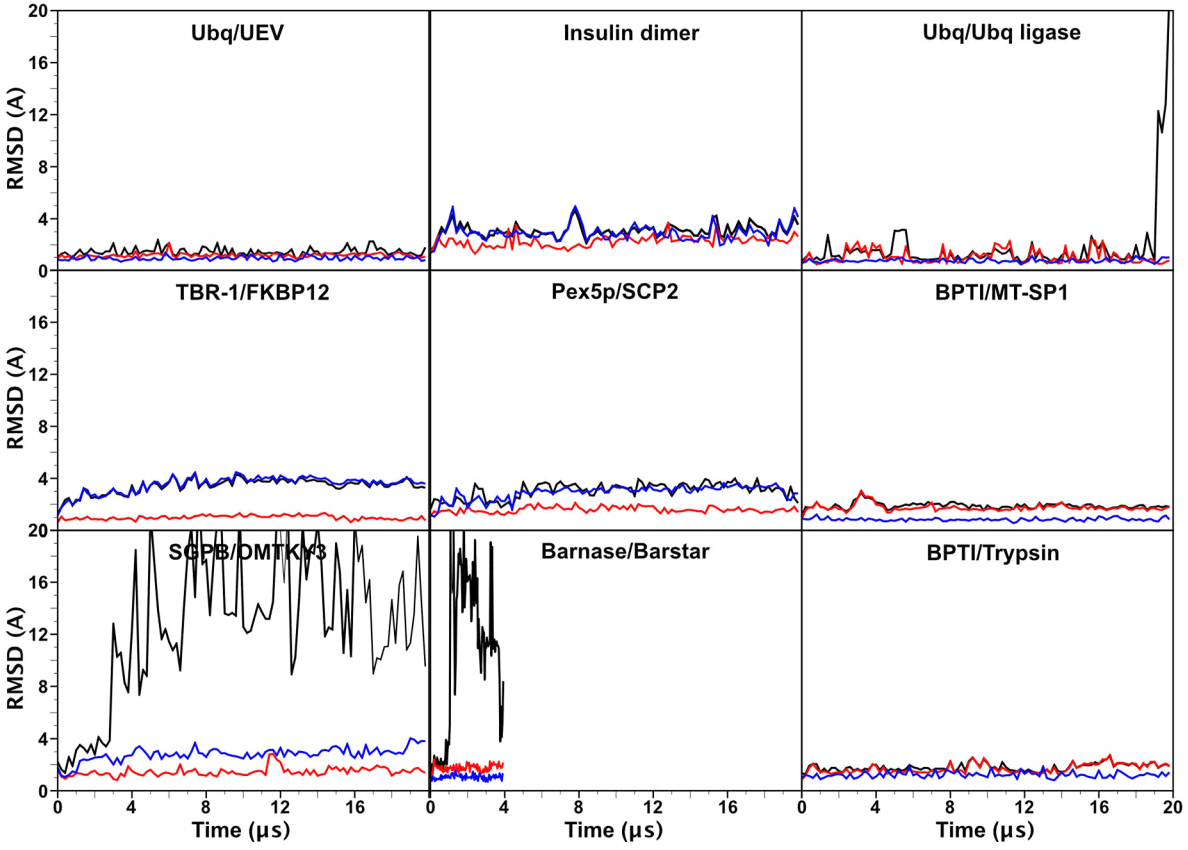

Figure 1. Cα-RMSD time series plots obtained from 20-μs MD simulations of nine protein−protein complexes using a99SB-*disp*. For each complex, the RMSD of each protein monomer is reported in red and blue; the RMSD of the complex is reported in black.

component systems. This is of particular concern for these state-of-the-art force fields, since the balance between those interactions occurring within water, between water and protein, and within the protein has been adjusted to achieve a higher degree of accuracy in the simulation of disordered protein systems.

Here, we first assess whether state-of-the-art force fields tuned to optimally describe both ordered and disordered states can also describe protein−protein complexes with a comparable level of accuracy. We performed simulations of nine different protein−protein complexes and observed substantial deviations from the starting experimental structure in a number of cases. We speculate that these complexes are stabilized by certain forces, such as those arising from charge−charge or charge−dipole interactions, that play a more limited role in defining the structure and dynamics of monomeric protein

https://dx.doi.org/10.1021/acs.jctc.9b00251
J. Chem. Theory Comput. 2020, 16, 2494−2507

systems. Our hypothesis implies that the description of protein−protein complexes can clearly not be improved by the intramolecular torsion-parameter optimization alone: An optimization of nonbonded-interaction parameters would also be required.

We performed such an optimization, based on both quantum mechanical (QM) and experimental data. Starting from one variant of the Amber protein force field,[12] we first fit backbone partial-charge and Lennard-Jones (LJ) parameters to reproduce interaction energies from several thousand QM calculations; subsequently, we optimized backbone torsion parameters to reproduce the residue-specific Ramachandran maps[13] observed in coil libraries[14] extracted from the Protein Data Bank (PDB) and then further refined these torsion parameters based on fitting to experimental data on the helical propensity of individual residues.[15] For side chains, we optimized torsion parameters based on fitting to a combination of QM data and data on the distributions of side-chain conformational preferences from the PDB[13,16] and refined the nonbonded parameters associated with side chains and ions to reproduce experimental data on osmotic coefficients[17−19] and Kirkwood−Buff integrals (KBIs).[20−22]

We show here that the resulting force field, which we name *DES-Amber*, is suitable for the simulation of small peptides, proteins, and protein−protein complexes and that, among other things, it can be used for the refinement of homology models to atomic resolution. Although DES-Amber represents a significant improvement for most of the systems studied, we note that the association free energies for protein complexes still often deviate by several kcal mol^{-1} from the experimentally determined values, possibly due to fundamental limitations in the functional form of nonpolarizable force fields of the sort typically used for biomolecular simulation.

RESULTS

Benchmark Simulations of Protein−Protein Complexes. We first assessed the ability of state-of-the-art force fields to describe the structures of protein complexes by performing MD simulations of nine different complexes (Table 1) that were selected to include a variety of interactions that can be found at the protein−protein interface (e.g., salt bridges, hydrogen bonds, and hydrophobic interactions) and a range of association constants spanning ∼7 orders of magnitude (between 100 μM and 10 pM, Table S13). We performed two independent 20-μs simulations for each system using a recently developed force field, a99SB-*disp*,[1] that provides descriptions of both folded and disordered protein states to a similar degree of accuracy, and the deviation from the experimental structure was measured. We also calculated, for some of the complexes, the association free energies using an enhanced sampling approach.[23]

Although all of the individual proteins appeared to be fairly stable in simulation (root-mean-square deviation (RMSD) from the X-ray structure of 1−4 Å), we found that three of the complexes became unstable and eventually dissociated during the 20 μs of simulation (Figure 1). (We obtained similar results (Table S13) using two other force fields (RSFF2+[10] and CHARMM36m[5]) optimized to perform well on both ordered and disordered proteins.) For a99SB-*disp*, the dissociation events observed in simulations of three of these complexes are inconsistent with experimentally measured dissociation times (in the range of 10^{-4} s to 10^{7} s; Table S13) that suggest that these complexes should be stable on the microsecond time scale. Dissociation events were not observed in simulations performed using a99SB*-ILDN,[16,24,25] which is designed to be used with TIP3P-like water models. This force field, like the recently developed Amber-FB15,[26] strongly favors collapsed structures (Figure S12), thus leading to more stable protein complexes; structural ensembles for disordered systems, however, are also highly compact, a result that disagrees with experiment and makes a99SB*-ILDN unsuitable for describing disordered protein systems (Table S13).

To further quantify this discrepancy, we attempted to calculate the association free energies using a variant of the method proposed by Doudou et al.[27] Although we found it challenging to obtain robust association free energy estimates for all of the systems, the calculated values correlated poorly with the experimental values. In certain cases, the free energies were severely underestimated (Table 1 and Figure 5), a result consistent with the observation that these complexes dissociate in equilibrium simulations on the microsecond time scale. This severe force field deficiency is likely the result of a poor description of certain interactions between macromolecules and, thus, cannot be addressed by torsion-parameter optimization alone: Some degree of reparameterization of the nonbonded interactions was thus required.

Force Field Optimization. We selected the a99SB-*disp* force field, which performed very well on both folded and disordered proteins, as the starting point for our force field reparameterization (we believe that CHARMM36m force field would have been an equally appropriate choice). The only difference between the a99SB-*disp* and Amber99[12] nonbonded parameters is a single additional LJ-pair interaction parameter. Initial tests indicated that this additional force field parameter does not impact our ability to fit the QM data, so it was eliminated, resulting in a starting set of nonbonded parameters that was equivalent to those in Amber99. Although the primary objective was to modify the nonbonded parameters, such reparameterization usually has some impact on the torsional degrees of freedom. The force field optimization was thus carried out in stages: The nonbonded parameters were modified first, and then the torsion parameters were optimized to be compatible with the new set of nonbonded parameters. In the few cases where torsion parameters were found to influence the nonbonded-parameter optimization, we iterated on the optimization cycle until self-consistency was achieved.

Backbone Nonbonded Parameters. As a first step, we determined a set of partial-charge and LJ parameters for the backbone atoms by fitting a data set containing 10 599 counterpoise-corrected interaction energies for *N*-methylacetamide (NMA) and Ace-Gly-Nme (GLY) dimers calculated at the MP2 level of theory with a quadruple-ζ basis set (more specifically, DF-MP2/aug-cc-pVQZ) using Molpro.[28] The dimer conformations used in the QM calculations were derived from structures observed in the PDB for residues in helices, sheets, and coils. Each data point, i, was weighted by $w_i = e^{-0.5E_{FF,i}} + e^{-0.5E_{QM,i}}$, where $E_{FF,i}$ is the force field energy, $E_{QM,i}$ is the QM energy, and the root-mean-square error (RMSE) between the force field and the QM dimer interaction energies was minimized. We made some attempts to add virtual sites to improve the description of hydrogen bonding, but we ultimately determined that there was not a large enough improvement in the fit to the QM data to justify their use in this context. The charges and the LJ parameters were optimized simultaneously, as the accurate representation of

https://dx.doi.org/10.1021/acs.jctc.9b00251
J. Chem. Theory Comput. 2020, 16, 2494−2507

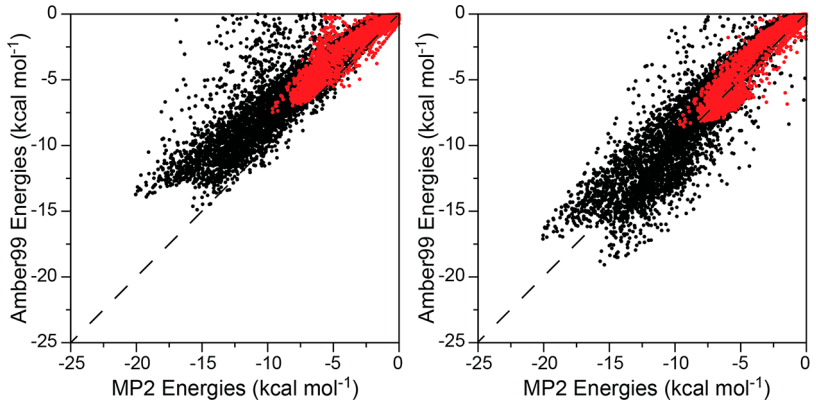

Figure 2. Interaction energies (kcal mol^{-1}) for NMA (red) and GLY2 (black) dimers calculated using the standard Amber99 force field (A) and after the nonbonded parameter optimization (B) compared to the reference MP2 data.

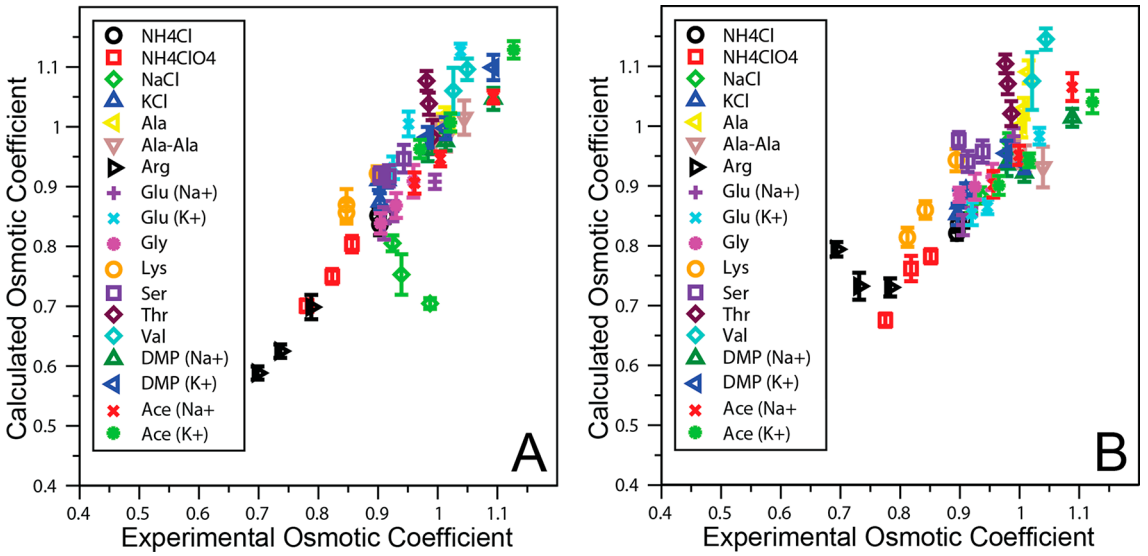

Figure 3. Comparison between the simulated and the experimental osmotic coefficients for the organic and inorganic salts used for the optimization of the side chain and ion nonbonded parameters. Best fits for scaling factors of 0.9 (DES-Amber, panel A) and 1.0 (DES-Amber SF1.0, panel B) are displayed. Error bars for the coefficients calculated from MD simulations were estimated using blocking.

short-range interactions requires the optimization of both the charge distribution and the shape of the LJ repulsive potential.

The original Amber99 nonbonded parameters correlate reasonably well with the QM data (Figure 2A), and indeed, simulations based on these parameters can be highly accurate, in particular for folded proteins.[3,7,8] The interaction energies are, however, generally underestimated with respect to the QM values (RMSE = 7.2 kcal mol^{-1}, Figure 2A), and this systematic error is corrected by the optimization (RMSE = 2.3 kcal mol^{-1}, Figure 2B). As a cross-validation to assess the performance of the optimized parameters on a more complex system, we calculated interaction energies for a set of 984 NMA trimers that were not part of the fitting data set. We found that the optimized parameters also reduced the error for NMA trimers from 4.2 kcal mol^{-1} to 1.4 kcal mol^{-1} when compared to QM-calculated values (Figure S2). This result indicates that the description of more complex systems, where polarization may be important, is greatly improved when compared to the original Amber99 force field. The resulting nonbonded parameters are reported in Table S1.

Side-Chain Nonbonded Parameters. Side-chain nonbonded parameters were optimized using both data from QM calculations and experimental data in the form of KBIs[20,22,29] and osmotic coefficients.[17−19] We focused the optimization on the parameters associated with polar and charged residues—specifically, Ser, Thr, Asp, Glu, Arg, and Lys—as interactions involving these residues can be crucial for the stability of protein−protein and protein−RNA complexes, but such interactions may be less important than hydrophobic interactions for the stability of folded proteins (and hence less extensively probed by previous studies of force field accuracy). For Ser and Thr, the relative stability of different hydrogen-bonding geometries is poorly reproduced by the Amber99 force field (Figure S1A,B). We thus used QM data to guide the selection of a charge distribution that would correctly rank the stability of the different hydrogen-bonding patterns (Figure S1A,B) while, at the same time, yielding simulations that were in agreement with experimentally derived KBI data for mixtures of water and ethanol (Figure S3).

The nonbonded parameters of the charged residues were refined to reproduce the osmotic coefficients of amino acid solutions at concentrations between 0.3 and 2 M. We initially fitted parameters for the monovalent ions Na^+, K^+, $NH4^+$, Cl^-, ClO_4^-, and dimethyl phosphate (DMP^-), using as a reference

https://dx.doi.org/10.1021/acs.jctc.9b00251
J. Chem. Theory Comput. 2020, 16, 2494−2507

osmotic coefficients for the following salts: NaCl, $NaClO_4$, sodium dimethyl phosphate (DMP Na^+), KCl, $KClO_4$, potassium dimethyl phosphate (DMP K^+), NH_4Cl, NH_4ClO_4, sodium acetate (Glu Na^+), and potassium acetate (Ace K^+) (Table S3). During this optimization, we discarded parameters that resulted in the positions of the first peaks of the ion−ion and ion−water RDFs deviating by more than 0.2 Å from the values estimated experimentally (Table S4). We subsequently determined parameters for the charged carboxyl and amino groups in amino acids by optimizing against glycine and alanine osmotic coefficients. These parameters were then fixed when optimizing the remaining side-chain parameters to match the osmotic coefficients of Ser, Thr, Val, Ala-Ala, Arg, Glu (Na^+), Glu (K^+), and Lys.

It has been argued that the local dielectric constant in fixed-charge force fields may be too low because they do not account for polarization effects and that, to effectively account for this deficiency, charges should be scaled.[30] During the optimization, we tested scaling the charges of ionic species using a number of scaling factors ranging from 0.75 to 1.0 and found that the two force fields with the best fit to the experimental osmotic coefficient resulted from scaling factors close to 1.0 (RMSE 0.068 using a scaling factor of 0.9 and 0.061 using a scaling factor of 1.0; see Figure 3). After extensive testing of these two force fields, we found that the force field obtained with a scaling factor of 0.9 for ionic charges performed slightly better in protein simulations (Tables S7 and S8). Results obtained with this force field, which we call *DES-Amber*, are thus discussed in the main text, whereas results obtained with a scaling factor of 1.0 (i.e., no rescaling of ionic charges), which we call *DES-Amber SF1.0*, are reported in the SI.

With a scaling factor of 0.9 (Figure 3A), only the results for NaCl at high salt concentrations (>0.5 M) deviate significantly from experiment. It has been shown that good agreement with experiment can be obtained for this salt by introducing a specific Na−Cl nonbonded LJ pair parameter.[19] Although introducing specific nonbonded LJ pair parameters for the ions can improve agreement with experimental data, the number of free parameters would greatly increase, and the size of the data set would not be sufficient to avoid overfitting. Using a scaling factor of 1.0 and ion parameters similar to those proposed by Joung and Cheatham,[31] a good fit was obtained to the NaCl osmotic coefficients, but we found it more problematic to fit the experimental data for arginine (Figure 3B). It is also worth noting that the LJ parameter optimizations in DES-Amber and DES-Amber SF1.0 led to somewhat different sets of LJ parameters (Table S2).

Torsion Parameters. Changes in nonbonded parameters do not directly affect the bond and angle terms but do influence the torsional degrees of freedom, because, in the Amber force field, 1−4 interactions are scaled but not excluded. We thus included refinement of the backbone and side-chain torsion parameters in our force field optimization.

Side-chain χ_1 torsion parameters were refined by using the results of MD simulations of A_4XA_4 peptides (with the backbone atoms restrained to a helical conformation) to iteratively fit the torsion parameters such that the g+, g−, and trans rotamer populations observed in simulation matched the populations observed in the PDB for peptides in helices[32] (Table S5). The helical state was chosen because it tends to be more structurally homogeneous than either the sheet or the coil states. During the optimization, to avoid unphysical results in low-population regions, torsion potentials were also weakly restrained to MP2-level QM potentials obtained from torsion scans of blocked amino acids.

For the optimization of the protein backbone torsion parameters, inspired by previous work,[13] we decided to develop residue-specific torsion potentials. Starting from the original Amber99SB torsions,[24] we optimized residue-specific ϕ and ψ torsion parameters so that the Ramachandran map obtained from a 1-μs simulation of a single blocked amino acid in water would match the Ramachandran map constructed for the same amino acid from a coil library of conformations extracted from high-resolution structures in the PDB.[13,14,33,34] As this procedure may be prone to overfitting, after determining the residue-specific torsions we averaged the torsion parameters across sets of residues with chemically similar Cγ side-chain atoms (Trp, Phe, and Tyr; Glu, Gln, Met, Lys, Arg, and Leu; Ile and Val; Asp and Asn), resulting in a total of 11 different sets of backbone torsion parameters. It is reassuring that this aggregation of torsion parameters does not significantly degrade the fit to the distributions obtained from the coil library (average similarity[13] coefficient for 20 torsions = 0.93, for 11 torsions = 0.92), as residues with chemically similar Cγ atoms are apparently characterized by similar corrections. Interestingly, one of the residues most different from any other residue is Ala, the only amino acid besides Gly that does not have a heavy atom in the γ position, suggesting that Ala may be a poor reference for optimizing residue-independent backbone torsion parameters.

The final step of torsion-parameter optimization involved adjusting the relative depth of the α-basin in the Ramachandran map to reproduce the experimentally observed propensity of each residue to form helices.[15] To this end, we performed 20-μs simulated tempering simulations with peptides of sequence Ace-$(AAXAA)_3$-Nme, and the ϕ and ψ backbone torsion parameters were refined until the Lifson-Roig helix extension parameters[35] at three different temperatures (278, 298, and 333 K) were consistent with the experimental estimates (Figure 4 and Table S6).[36] These adjustments to the backbone torsion potential usually amounted to a few tenths of a kcal mol^{-1} or less and had a very small impact on the fit to the PDB coil library (average similarity coefficient = 0.91), as the helical basin is not highly populated in this data set.

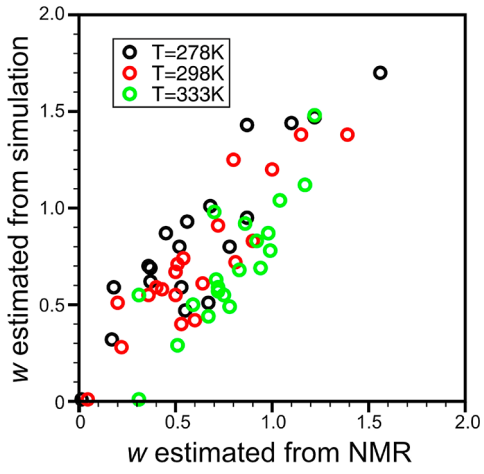

Figure 4. Comparison between the Lifson-Roig helix extension parameters w for the 20 amino acids estimated from simulation and NMR experiments[36] at three temperatures: 278, 298, and 333 K.

https://dx.doi.org/10.1021/acs.jctc.9b00251
J. Chem. Theory Comput. 2020, 16, 2494−2507

Assessment of DES-Amber Accuracy. We examined the ability of DES-Amber to accurately reproduce a wide range of experimental data. In addition to the Robustelli et al. benchmark,[1] we also tested the ability of the force field to produce stable simulations of 52 proteins from the Mao[37] and Huang[5] data sets and 9 additional protein−protein complexes; to fold 13 small proteins[38,39] and one protein−protein complex;[40] to predict the relative stability of 22 Trp-cage mutants; and to refine 6 homology models.

The Robustelli Benchmark. The Robustelli et al. benchmark has been described in detail elsewhere.[1] It is composed of 21 proteins and over 9000 NMR and SAXS experimental measurements and can be used to evaluate the ability of a force field to describe the structural dynamics of ordered and disordered proteins. Overall, we find that DES-Amber reproduces the structural properties of both ordered and disordered proteins at a level of accuracy comparable to a99SB-*disp* (Table 2), the force field that was previously found to exhibit the best performance on this benchmark.[1]

In particular, simulations run with DES-Amber, on average, showed slightly improved agreement with experimental measurements for the folded proteins ubiquitin, Gb3, BPTI, and HEWL when compared to simulations run with a99SB-*disp*. The most striking improvement was seen in the agreement with backbone RDCs (Table S7). DES-Amber also showed substantially improved agreement with the backbone RDCs of the ordered domains of calmodulin (Q-factors 0.19 and 0.24 for the N-terminal and C-terminal domains in simulations run with DES-Amber, compared to Q-factors of 0.22 and 0.39 in simulations run with a99SB-*disp*). These results suggest that the refinement of torsion parameters based on PDB coil-library distributions can result in more accurate descriptions of average conformational preferences in simulations of folded protein domains.

Simulations of disordered proteins run with DES-Amber showed, on average, slightly worse agreement with experiment when compared to simulations run with a99SB-*disp* (Table S9), with DES-Amber simulations producing slightly more compact structures (Table S10). Radii of gyration (R_g's) observed in simulations performed with DES-Amber had an average error of 10% compared to experimental values, whereas simulations performed with a99SB-*disp* had an average error of 5%. DES-Amber simulation results did, however, show better agreement with experimental backbone scalar couplings than did results from a99SB-*disp* simulations (Table S9). These findings suggest that the torsion-parameter refinements based on PDB coil-library distributions can also improve the local sampling of dihedral angles in disordered proteins.

Simulations performed with DES-Amber resulted in substantially more β structure than did simulations performed with a99SB-*disp*, consistent with the fact that more pronounced β basins were observed when torsion parameters were refined using PDB coil-library data. It is also clear that increased β-hairpin formation accounts for the more compact conformations observed in simulations performed with DES-Amber (Figure S6). Due to the presence of a larger amount of metastable β-hairpin structure in DES-Amber, 60-μs simulations were required to observe multiple association and dissociation events of β hairpins and achieve reasonably converged estimates of β-hairpin propensities and R_g's, as indicated by the error estimates obtained using blocking on the R_g and secondary structure content (Figure S6). We note that while the error estimates presented here suggest that the formation and disassociation of the β hairpins observed in these simulations were reasonably well sampled, we cannot rule out the possibility that longer simulations would explore other conformations stable on longer time scales. Simulated tempering simulations of CLN025, trpzip1, and the GB1 hairpin showed substantially elevated populations of hairpin structure compared to simulations performed with a99SB-*disp*, as well as closer agreement with experimental melting curves (Figure S9).

We note that, for the N_{TAIL} domain of the Sendai virus nucleoprotein,[41] a simulation with DES-Amber reproduced the helix observed experimentally in a region where no helix was found in a simulation with a99SB-*disp*, possibly an indication that fitting torsion parameters to reproduce Lifson-Roig helix propensities leads to an improved description of residual secondary structure elements in disordered proteins (Figure S7).

Stability of Salt Bridges. To assess the accuracy of salt bridge interactions, we performed 10 μs of simulation of GB1 and calculated the stability of salt bridge interactions using the definition of ref 42. There are three salt bridges in the X-ray structure of this protein (Lys_{12}-Glu_{23}, Lys_{39}-Asp_{35}, and Lys_{58}-Glu_{55}).[43] These salt bridges are solvent exposed, and NMR measurements indicate that they should form rarely in solution.[44] In most force fields these salt bridges form, on

Table 2. Normalized Force Field Scores (see Methods) for Folded Proteins, Disordered Proteins, the Partially Disordered Dimer GCN4, and Calmodulin, Which Contains Two Folded Globular Domains Connected by a Flexible Linker[a]

	DES-Amber	DES-Amber SF1.0	a99SB-*disp*
Folded Proteins			
ubiquitin	1.46	1.47	1.37
Gb3	1.05	1.03	1.44
BPTI	1.16	1.15	1.04
HEWL	1.06	1.06	1.15
average	*1.18*	*1.18*	*1.25*
Disordered Proteins			
drKN	1.13	1.65	1.19
ACTR	1.26	1.50	1.18
N_{TAIL}	1.48	1.58	1.01
α-synuclein	1.11	1.83	1.28
PaaA2	1.19	1.37	1.35
Aβ40	1.40	1.49	1.28
$p15^{PAF}$	1.18	1.58	1.06
Sic1	1.32	1.27	1.31
Ash1	1.14	1.23	1.24
average	*1.25*	*1.50*	*1.21*
Partially Disordered Dimer			
GCN4	1.52	3.03	1.04
Multi-Domain Protein			
calmodulin	1.01	1.32	1.22

[a]A normalized force field score of 1 indicates that a force field produces the closest agreement with experiment among all of the force fields tested. Force field scores were calculated by considering simulations run with DES-Amber and DES-Amber SF1.0, as well as previously reported simulations[1] run using a99SB-*disp*, a99SB*-ILDN/TIP3P, c22*/TIP3P, c36m/TIP3P, a03ws, and a99SB-ILDN/TIP4P-D, for each type of experimental observable considered for a given system. Force field scores are reported here for DES-Amber, DES-Amber SF1.0, and a99SB-*disp*.

https://dx.doi.org/10.1021/acs.jctc.9b00251
J. Chem. Theory Comput. 2020, 16, 2494−2507

average, 50−77% of the time,[42] suggesting that this interaction is typically overestimated in simulation. The average population in simulations performed with DES-Amber is 45% (Lys_{12}-Glu_{23} 54%, Lys_{39}-Asp_{35} 59%, and Lys_{58}-Glu_{55} 24%), in better agreement with experiment. Importantly, in the DES-Amber simulation, the most stable salt bridge was Lys_{39}-Asp_{35}—in agreement with experiment[44]—a feature not captured by a99SB-*disp* and other commonly used force fields that predict this salt bridge to be the weakest of the three.[42]

Stability of Folded Proteins and Protein−Protein Complexes. In addition, we performed MD simulations of the 14 folded proteins that are part of the Huang et al. set[5] and of the 9 protein−protein complexes used in our initial assessment, with the goal of verifying that the structures determined by X-ray crystallography would be maintained during a 20-μs simulation (Figures 5 and S10). We also used DES-Amber to predict NOE and chemical shift data for the 41 proteins in the Mao et al. set[37] and found that the results are at a level of accuracy comparable to or exceeding that of a99SB-*disp* (Table S7). All systems remained stable in these simulations. The only protein that displayed a substantial degree of conformational flexibility was the C-terminal domain of the RAP74 subunit of the human transcription factor IIF (1I27 in Figure S10), a zinc-binding protein with a long, flexible tail that was also found to be highly flexible in a previously published study using the CHARMM force field.[5]

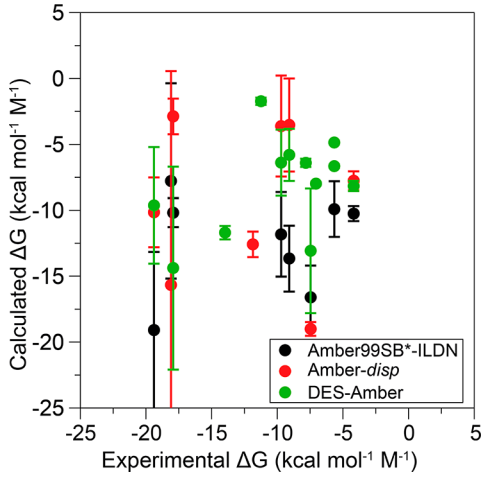

Figure 5. Comparison of calculated and experimental association free energies calculated for a number of protein complexes using a99SB*-ILDN, a99SB-*disp*, or DES-Amber. For the complexes for which values could be obtained using two different restraint sets, the average and standard deviation of the two measurements are reported. In the other cases, the error estimated using blocking is reported.

In contrast to the results obtained using the a99SB-*disp* force field, none of the protein−protein complexes dissociated (Figure S11) in 50 μs of simulation performed using DES-Amber, suggesting that the reparameterization of the non-bonded parameters achieved the goal of improving the description of these systems. To quantify the level of improvement, we attempted to calculate association free energies for these complexes (Table 1 and Figure 5). As in the case of a99SB-*disp*, we were unable to robustly calculate association free energies for some of the systems, and there is a large degree of uncertainty in the calculated values, due to the difficulty of obtaining well-converged results. The results obtained for the systems where we were able to compute association free energies suggest that, although the RMSD from the experimentally measured association free energies is lower in DES-Amber (5 kcal mol^{-1} M^{-1}) than in a99SB-*disp* (8 kcal mol^{-1} M^{-1}), the association free energies still correlate poorly with the experimental values. We conclude that DES-Amber is suitable for describing the structure and dynamics of both ordered and disordered states of single-chain proteins and of many protein−protein complexes on the tens-of-microseconds time scale, but that further improvements will be required to reproduce the association free energy of protein complexes with chemical (sub-kcal mol^{-1}) accuracy.

Fast-Folding Proteins. As an additional test, we also evaluated the ability of DES-Amber to recapitulate the experimentally determined native states for 9 fast-folding proteins[38,39] and 1 protein−protein complex.[40] We performed a 1 ms simulated tempering[45] simulation for each of the 9 proteins, starting from an extended state with temperatures ranging from 278 to 410 K. Structures closer than 2 Å Cα RMSD from the folded state were reached multiple times in most simulations (Figure S4). The folded state for NuG2 was not sampled in the simulated tempering run. Test simulations indicated that the native state of NuG2 was thermodynamically quite stable, and the protein folded after ∼500 μs of NPT simulation at 360 K (Figure S4), a temperature at which

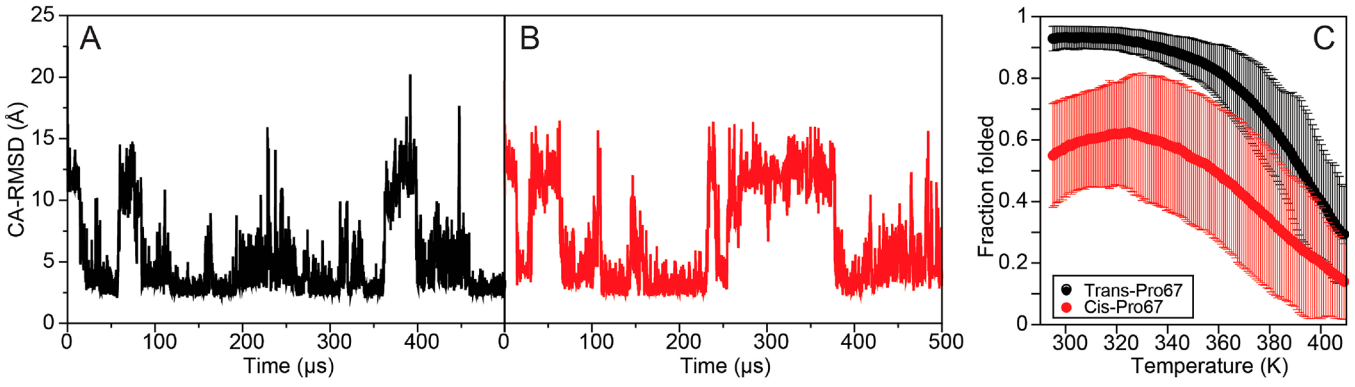

Figure 6. RMSD from the experimentally determined structure (PDB ID: 1KBH[40]) in simulated tempering simulations of the ACTR/NCBD complex started from an unbound state with the backbone of proline 67 either in the trans- (A) or in the cis- (B) conformation. The thermal stabilities of the complex for the trans- (black) and cis- (red) isomers are reported in (C). The folded segments of the trajectory are defined using a dual-cutoff approach[38,67] on the Cα RMSD with cutoffs of 3 Å for the folded state and 10 Å for the unfolded state.

https://dx.doi.org/10.1021/acs.jctc.9b00251
J. Chem. Theory Comput. 2020, 16, 2494−2507

folding of this protein is expected to be fastest. Based on this result, we conclude that folding was not observed in the simulated tempering run due to the slow folding time, rather than to folded-state instability. In the case of BBL, a three-helix bundle, although helical conformations with the correct topology were often sampled in the simulation, conformations closer than 2 Å Cα RMSD from the experimentally determined folded state were reached only transiently, as this protein domain is highly flexible. We note that BBL had been shown to be particularly problematic in previous ab initio protein folding studies that used different force fields,[38,46] suggesting that this protein may be particularly sensitive to even relatively minor force field inaccuracies.

Folding enthalpies and heat capacities were estimated from the simulated tempering simulations as the difference in potential energy between the folded and unfolded state.[47] We found this approach to converge faster than using the van't Hoff equation, but the two methods give the same results, within statistical error. Although the calculated heat capacities agree well with experimental values, folding enthalpies at 300 K were generally underestimated compared to the experimental values (Table S15). The origin of this discrepancy, which has been observed previously with other state-of-the-art force fields,[1,48] is unclear.

We also simulated the folding-upon-binding of the complex between the p160 transcriptional coactivator (ACTR) and the nuclear coactivator binding domain (NCBD).[40] Starting from an unbound structure, the experimentally determined structure was readily recapitulated as the most stable structure in the simulated tempering run (Figure 6A). It has recently been shown that the cis−trans isomerization of proline 67 in the NCBD destabilizes the complex, giving rise to a rather distinct kinetic phase in folding experiments.[49] Our simulations of complex formation that began with proline 67 in a cis conformation reached a structure consistent with the one determined experimentally (Figure 6B). In these simulations, however, two of the terminal hydrogen bonds stabilizing helix 1 in the NCBD were unable to form due to the geometric constraints imposed by the cis peptide bond, and thus the complex was ∼1.5 kcal mol^{-1} less stable at 310 K than the complex was in simulations with the trans isomer (Figure 6C). This difference corresponds roughly to a 1:10 population ratio between the cis and the trans isomers, respectively, and is in good agreement with the experimental estimates of a 1:8 ratio.[49]

Thermodynamics of Trp-cage Mutants. To better assess whether the intricate balance between different types of interactions is faithfully reproduced by DES-Amber, we examined the ability of the force field to reproduce the relative stability of 22 mutants of Trp-cage by performing a 200-μs equilibrium simulation for each mutant in order to observe reversible folding events. In each of these simulations, we observed 35−169 folding events (a folding event is defined as a transition from a Cα RMSD above 6 Å to a Cα RMSD below 0.8 Å), depending on the particular mutant, allowing us to estimate the folding free energy of each mutant to within a statistical error of <0.2 kcal mol^{-1}. We found that the relative folding free energies for 231 pairs of sequences agreed well with experimental estimates,[50−55] with an overall RMSE of 0.5 kcal mol^{-1} (Figure 7), suggesting that DES-Amber provides a reasonable description of the relative strength of the different interactions that stabilize the folded conformations of proteins.

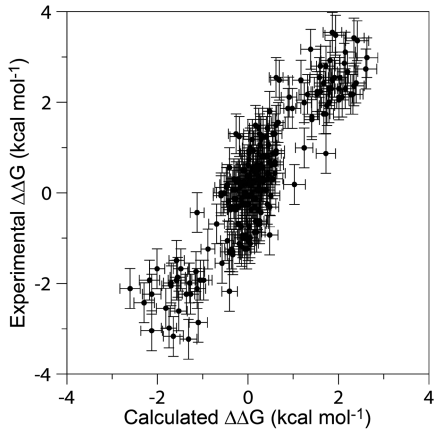

Figure 7. Comparison of the simulated relative folding free energies of 231 pairs of Trp-cage sequences with the experimentally determined[50−55] relative stabilities.

Homology model refinement. Finally, we examined the extent to which DES-Amber may be suitable for homology model refinement. To this end, we selected six refinement targets from the CASP11[56] and CASP12[57] experiments (TR782, TR821, TR829, TR872, TR921, and TR944) based on the criteria that the proteins: (i) are monomeric, (ii) do not bind metal ions or cofactors, and (iii) do not contain disordered regions larger than 10 amino acids in length. For each target, we performed 200 μs of simulated tempering, with flat-bottom backbone RMSD restraints to the homology model backbone structure for residues in helical or β-sheet conformations, as determined using STRIDE.[58] We performed a cluster analysis of the last 100 μs of each simulation and selected the center of the most populated cluster as the representative structure. In four out of six cases (TR782, TR821, TR829, and TR872), the representative structure was closer to the experimental structure than the starting structure, indicating a successful refinement (Figure 8). In one case (TR921), the representative structure remained close to the starting structure (i.e., no refinement), and in one case (TR944) the simulation moved away from the experimental structure (Figure 8). The successful refinements are of quality comparable to the best refinements reported for each target in the CASP experiments,[56,57] suggesting that the DES-Amber force field may be suitable for performing MD-based homology model refinement in structure-prediction experiments.

■ DISCUSSION AND CONCLUSIONS

We have described the development and validation of DES-Amber, a force field based on the refinement of both torsion-angle and nonbonded parameters to a combination of QM and experimental data. The results of validating DES-Amber against a large number of previously studied and new benchmark systems suggest that DES-Amber can describe ordered and disordered proteins with a level of accuracy comparable to that of the best force fields available, while at the same time providing a slightly improved description of protein−protein complexes. The DES-Amber force field is suitable for folding fast-folding proteins from extended conformations and provides a more balanced description of the relative strength of the different interactions that stabilize the folded conformations of proteins. Simulations based on this force field also improved homology models in four out of six cases investigated.

https://dx.doi.org/10.1021/acs.jctc.9b00251
J. Chem. Theory Comput. 2020, 16, 2494−2507

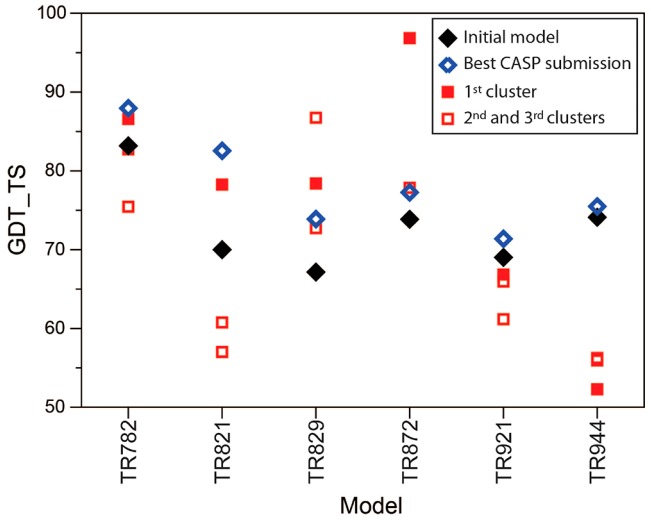

Figure 8. Refinement of six homology models from the CASP11 and CASP12 experiments using MD simulations performed with the DES-Amber force field. For each refinement target, the GDT score[103] of the initial model is reported as a black diamond; the GDT score of the average structure of the most populated cluster obtained in the simulated tempering simulation is reported as a filled red square, and the scores of the average structures of the second and third clusters are reported as empty red squares. For comparison, the GDT scores of the best CASP submissions for each target are reported as blue diamonds.

Although DES-Amber represents an improvement in many respects over previous state-of-the-art force fields and achieves a satisfactory level of accuracy in many cases, association constants of protein complexes in DES-Amber simulations correlate poorly with experimental data (Figure 5), in particular for systems characterized by highly polar interfaces. Visual inspection of the simulation of the barnase−barstar complex, for example, reveals that a number of water molecules entered the protein−protein interface within the first few microseconds of simulation. Although the distortion in terms of global RMSD was relatively small (<2 Å, Figure 5), some key, direct charge−charge interactions were disrupted in the process.

Several lines of evidence suggest that solvent-exposed charge−charge interactions are reasonably well described by the DES-Amber force field. Predicted osmotic coefficients for Arg and Glu salts are in good agreement with experimental values, for example, and the strength of salt bridges in GB1, while still slightly overestimated,[44] is more in line than previous force fields with the experimental data.[42] Furthermore, simulated folding free energy changes upon mutations of charged amino acids in the Trp-cage protein agree, to within statistical error, with experimental results (Table S9). In DES-Amber simulations of protein complexes, however, many of the interactions involving charged residues were buried at the protein−protein interface rather than solvent-exposed. We suspect that the intrinsic limitations of the functional form of DES-Amber and other nonpolarizable force fields may prevent us from achieving a higher level of accuracy for interactions involving charged groups in these very different dielectric environments (solvent-exposed versus buried at a protein−protein interface). The development of polarizable force fields is an active area of research,[59−63] and these systems could be examples for which polarization will be required to achieve a substantially higher degree of accuracy.

METHODS

Optimization of Backbone Nonbonded Parameters. QM calculations were used to provide reference data for fitting the backbone nonbonded parameters. To this end, binding energies were calculated at the density-fit MP2[64] level of theory (with a quadruple-ζ basis set) using MolPro[28] for 6629 Ace-Gly-Nme dimers and 3970 *N*-methylacetamide dimers. Dimer conformations were generated by extracting, fragmenting, and clustering backbone structures taken from the PDB. About 30% of the data correspond to distance-based scans initiated from one of these conformations. Fitted parameters were the C_{12} and C_6 Lennard-Jones coefficients and partial charges of the C, O, N, H, Cα, and Hα atoms. A Monte Carlo search in parameter space was used to find the parameter set with the lowest weighted RMSD from the QM data.

Calculation of Kirkwood-Buff integrals. Kirkwood-Buff integrals (KBIs) were calculated for ethanol−water solutions with mole fractions ranging from 0.05 to 0.98 and compared to values derived experimentally.[65] Simulations were set up in 80−90-Å periodic boxes. For each mixture, 50 ns simulations were performed in the NPT ensemble using the DES-Amber force field and the TIP4P-D water model. The KBIs were calculated from the integrals of the water−water, water−ethanol, and ethanol−ethanol radial distribution functions.

Calculation of Osmotic Coefficients. Osmotic coefficients were calculated for the following solutes: NaCl, KCl, NH_4Cl, NH_4ClO_4, DMP Na^+, DMP K^+, Ace Na^+, Ace K^+, sodium glutamate (Glu Na^+), potassium glutamate (Glu K^+), arginine chloride (Arg), lysine chloride (Lys), alanine (Ala), dialanine (Ala-Ala), glycine (Gly), valine (Val), serine (Ser), and threonine (Thr) (Table S3). For each system, 32 solute molecules were solvated in TIP4P-D water in a 90-Å periodic box. A flat-bottom harmonic constraint was applied to the center of mass of each solute molecule, with the center of the periodic box as reference and a force constant of 10 kcal mol^{-1} $Å^{-1}$. Simulations of 500 ns were performed in the NPT ensemble at three different concentrations of 0.5, 1.0, and 2.0 M by varying the distance associated with the flat-bottom restraints. Due to their lower solubility, valine simulations were performed at 0.3 and 0.6 M, and dialanine and DMP simulations were performed at 0.3, 0.6, and 1.0 M. Osmotic pressures were calculated from the mean force on the constraint.[19] Using NaCl as a test system, we verified that this approach gives results identical to previous studies in which a flat-bottom harmonic constraint was only applied to one of the box directions.[18,19,66] Ammonia was parametrized using the same LJ parameters and partial-charge distribution as protonated amines; the same LJ parameters and similar charge distributions were used for all carboxylic groups.

Calculation of Lifson-Roig Helix Extension Parameters. Twenty peptides of sequence Ace-$(AAXAA)_3$-Nme were solvated in 40-Å periodic boxes containing ∼2000 water molecules. For each system, 20 μs of simulated tempering simulations were performed with 30 temperature intervals spanning a temperature range from 273 to 380 K. Lifson-Roig helix extension parameters[35] were calculated from the observed distributions of helical states, following the approach of Best and Hummer.[15,25] Residues were considered to form a helix if they were part of a stretch of three contiguous helical residues, which were defined as residues having backbone torsion angles

https://dx.doi.org/10.1021/acs.jctc.9b00251
J. Chem. Theory Comput. 2020, 16, 2494−2507

$-100° < \psi < -30°$ and $-7° < \phi < 67°$. We first determined the helix nucleation and extension parameters that best fit the observed distribution of helical fractions for Ace-$(A)_{15}$-Nme and then used these values for the fit of the helix nucleation and extension parameters of all other residues.

Calculation of Trp-Cage Mutational Free Energies. We selected 22 mutants of the Trp-cage miniprotein, with mutations spanning all nonglycine residues in the sequence (see Table S9 for a complete list). For each mutant, we performed a 200-μs MD simulation at 320 K starting from an extended state. The trajectory was partitioned into folded and unfolded states applying a dual-cutoff approach[38,67] to the Cα RMSD time series with cutoffs of 0.8 Å for the folded state and 6.0 Å for the unfolded state. The rather tight cutoff for the folded state was necessary to exclude misfolded structures. We found, however, that the results were only very weakly dependent on the exact value of this cutoff. The folding free energy for each mutant was calculated based on the ratio of the folded fraction to the unfolded fraction observed in simulation (Table S9), and we used these free energies to compute 231 $\Delta\Delta G_{mut}$ (relative free energies of mutation) between all possible pairs of mutants. In cases in which the experimental folding free energies at 320 K were not directly available, we estimated them from the reported melting temperatures (T_m) using the relation $\Delta G_f = (T_m - 320) \times 0.062 \pm 5 \times 10^{-3}$ kcal mol^{-1}.[50] The experimental uncertainty was estimated as the larger of either the error arising from the uncertainty in the $T_m/\Delta G_f$ relationship or the difference between the T_m's measured with different methods.

Calculation of Normalized Force Field Scores. As in the original Robustelli et al. paper,[1] we here compare the relative accuracy of each force field on the Robustelli benchmark by calculating and reporting their normalized force field scores. For folded proteins, the RMSD from each class of experimental data (such as side-chain scalar couplings, RDCs, etc.) was normalized by the smallest observed RMSD among the following force fields: DES-Amber, DES-Amber SF1.0 (unscaled charges), a99SB-*disp*,[1] a99SB*-ILDN/TIP3P,[16,24,25] c22*/TIP3P,[68] c36m/TIP3P,[5] a03ws,[9] a99SB-UCB,[69] and a99SB-ILDN/TIP4P-D.[1,16,24] The normalized force field score (for folded proteins) was determined by taking the average of the normalized RMSDs over all classes of experimental measurements

$$\text{Folded Protein FF}_{\text{Score}} = \frac{1}{N}\sum_{i=1}^{N}\frac{\text{FF}_{\text{RMSD}}}{\text{RMSD}_{\text{Norm}}}$$

where N is the number of classes of experimental data considered, FF_{RMSD} is the RMSD of the simulated values from the corresponding experimental values for class i, and $\text{RMSD}_{\text{Norm}}$ is the smallest observed RMSD of all the nine force fields examined in this study for class i. In this metric, a normalized FF_{Score} of 1 indicates that a force field produces the closest agreement with experiment among all of the force fields tested for all of the classes of experimental observables considered.

For disordered proteins (GCN4 and calmodulin), force field scores were computed as a combination of a backbone NMR chemical shift score (CS_{Score}), a score based on additional NMR measurements ($\text{NMR}_{\text{Score}}$), and an R_g deviation penalty (R_{gPenalty}). The CS_{Score} was determined analogously to the folded-protein score by normalizing the RMSD for each class of chemical shift data by the smallest RMSD observed across the nine force fields and taking an average of the normalized RMSDs over all sets of experimental chemical shifts. The NMR score was computed analogously for all additional classes of NMR measurements. The R_{gPenalty} was 0 if the average simulated R_g was within the experimentally estimated error ($R_{\text{gExperror}}$). For deviations larger than the estimated experimental error, the R_{gPenalty} was calculated as

$$R_{\text{gPenalty}} = \frac{|R_{\text{gExp}} - R_{\text{gSim}}| - R_{\text{gExperror}}}{R_{\text{gExp}}}$$

The combined disordered-protein force field score was computed as

$$\text{Disordered Protein FF}_{\text{Score}} = \frac{\text{CS}_{\text{Score}} + \text{NMR}_{\text{Score}}}{2} + R_{\text{gPenalty}}$$

Calculation of Association Free Energies for Protein Complexes. The association free energies for protein−protein complexes were calculated based on an adaptation of the protocol proposed by Doudou et al. for the calculation of ligand-binding affinities,[27] which itself can be considered a variant of the method proposed by Roux and co-workers.[70,71] Each protein complex was rotated such that the vector connecting the centers of mass of the two proteins was aligned along the z-axis. Weak position restraints (force constant of 0.01 kcal mol^{-1} Å^{-1}) were applied to the x and y coordinates of the Cα atoms of residues involved in secondary structure elements, and restraints of 0.1 kcal mol^{-1} Å^{-1} were applied to the x and y coordinates of the Cα atoms of the interface loops. The potential of mean force (PMF) along the distance between the center of mass of the two proteins was then calculated using a simulated tempering approach with 600 rungs spanning 15 Å starting from the X-ray structure distance. The first 200 rungs were assigned to the bound state and the last 100 to the unbound state.

We estimated the effect of the position restraints (ΔG_R in eq 10 of ref 27) at 1-Å intervals along the PMF by performing 10-μs equilibrium unrestrained simulations of the isolated monomers and of the complex using the Bennett Acceptance Ratio[72] to calculate the free energy difference between the restrained and unrestrained simulations for all distances where there was overlap between the two probability distributions. As expected, this region always included the free energy minimum and its neighborhood. In the case of the monomer simulations, the calculation was performed between the unrestrained monomer simulations and the frames of the enhanced sampling dimer simulations in which the center of mass distance was at least 13-Å larger than the equilibrium value. We calculated the restraint energy as the product between the Cα RMSD (after alignment) with respect to the reference structure (weighted by the relative force constant applied to each atom and calculated on the x and y coordinates only) and the restraint force constant. Because the Cα-RMSD calculation imposes a particular rotation on the system, the energy corresponding to the three rotational degrees of freedom that were lost upon alignment (1.5 k_bT) was added to the free energy estimate.

During the simulated tempering run, the protein complexes formed and dissociated several times. The distance-based reaction coordinate and the very weak constraints used meant that the native bound pose was not always reached; in some

https://dx.doi.org/10.1021/acs.jctc.9b00251
J. Chem. Theory Comput. 2020, 16, 2494−2507

cases, the two proteins formed a complex that did not contain the correct native contacts. We defined a native conformation as a conformation in which >80% of the native Cβ−Cβ contacts (distance < 7 Å and maintained >95% of the time in a 10-μs unrestrained simulation of the complex) formed; free energies obtained from enhanced sampling simulations in which such conformations had not been observed after the first 5 μs of simulation should be considered highly unreliable and are reported in italics in Table 1. As a further test of reproducibility, for 10 of the systems described in Table 1, we repeated the PMF calculation using position restraints of 0.01 kcal mol^{-1} on all the Cα atoms, including the interface loops and excluding only the disordered tails. For most systems for which both enhanced sampling simulations reached the correct native state, the two calculations gave comparable results (Table 1). The last four systems in Table 1, which were not part of the initial benchmark, were added to verify that we were not overfitting to our initial benchmark. For these systems, association free energies were computed for DES-Amber using only a single protocol.

MD Simulation Setup. MD simulations were performed using the DES-Amber force field (as described in this paper) in combination with the TIP4P-D water model,[2] with the exception of the set of initial simulations used to assess the accuracy of existing state-of-the-art force fields in describing protein complexes, which were performed using the following: a99SB-*disp*[1] with TIP4P-D-1.6; RSFF2+[10] with TIP4P-D; and CHARMM36m[5] with TIP3P-CHARMM.[73] To gently relax any initial clashes, systems were equilibrated with restraints on the backbone atoms at 300 K and 1 bar for 100 ps using the Desmond software.[74] Folded proteins and protein complexes were further equilibrated for 1 μs on the Anton specialized hardware[75] with position restraints on the Cα atoms. Production runs in the NPT ensemble[76−78] were performed on the Anton specialized hardware with a 1:2 RESPA scheme.[79] Bonds involving hydrogen atoms were restrained to their equilibrium lengths using the M-SHAKE algorithm.[80] The Gaussian split Ewald method[81] with a 32 × 32 × 32 mesh was used to account for the long-range part of the electrostatic interactions. All simulations were run at 300 K, with the exception of $(AAXAA)_3$ peptides and the fast-folding proteins, where simulated tempering[45] was used to enhance sampling and calculate temperature-dependent properties. In simulated tempering simulations of the $(AAXAA)_3$ peptides and CLN025, 20 rungs were spaced geometrically spanning 278−390 K. In simulated tempering simulations of Trp-cage, K24nL_K29nL villin, and GTT, 60 rungs were spaced geometrically spanning 278−400 K. Simulated tempering simulations of the remaining fast-folding proteins were carried out using 100 rungs, spaced geometrically, spanning 278−410 K.

■ ASSOCIATED CONTENT

Supporting Information

The Supporting Information is available free of charge at https://pubs.acs.org/doi/10.1021/acs.jctc.9b00251.

DES-Amber force field parameters and additional data used for the validation and development of the force field (PDF)

■ AUTHOR INFORMATION

Corresponding Authors

Stefano Piana − *D. E. Shaw Research, New York, New York 10036, United States*; Phone: (212) 403-8165; Email: Stefano.Piana-Agostinetti@DEShawResearch.com; Fax: (646) 873-2165

David E. Shaw − *D. E. Shaw Research, New York, New York 10036, United States; Department of Biochemistry and Molecular Biophysics, Columbia University, New York, New York 10032, United States;* orcid.org/0000-0001-8265-5761; Phone: (212) 478-0260; Email: David.Shaw@DEShawResearch.com; Fax: (212) 845-1286

Authors

Paul Robustelli − *D. E. Shaw Research, New York, New York 10036, United States*

Dazhi Tan − *D. E. Shaw Research, New York, New York 10036, United States*

Songela Chen − *D. E. Shaw Research, New York, New York 10036, United States*

Complete contact information is available at: https://pubs.acs.org/10.1021/acs.jctc.9b00251

Author Contributions

§(S.P. and P.R.) These authors contributed equally to the manuscript.

Notes

The authors declare the following competing financial interest(s): This study was conducted and funded internally by D. E. Shaw Research, of which D.E.S. is the sole beneficial owner and Chief Scientist, and with which all authors are affiliated.

■ ACKNOWLEDGMENTS

The authors thank John Klepeis for helpful discussions and a critical reading of the manuscript; Alexander Donchev, Andrew Taube, and John Klepeis for sharing the QM data; Aditya Limaye and Brent Gregersen for sharing the code to calculate KBIs; and Berkman Frank for editorial assistance.

■ REFERENCES

(1) Robustelli, P.; Piana, S.; Shaw, D. E. Developing a molecular dynamics force field for both folded and disordered protein states. *Proc. Natl. Acad. Sci. U. S. A.* **2018**, *115* (21), E4758−E4766.

(2) Piana, S.; Donchev, A. G.; Robustelli, P.; Shaw, D. E. Water dispersion interactions strongly influence simulated structural properties of disordered protein states. *J. Phys. Chem. B* **2015**, *119* (16), 5113−5123.

(3) Lindorff-Larsen, K.; Maragakis, P.; Piana, S.; Eastwood, M. P.; Dror, R. O.; Shaw, D. E. Systematic validation of protein force fields against experimental data. *PLoS One* **2012**, *7* (2), No. e32131.

(4) Lange, O. F.; van der Spoel, D.; de Groot, B. L. Scrutinizing molecular mechanics force fields on the submicrosecond timescale with NMR data. *Biophys. J.* **2010**, *99* (2), 647−655.

(5) Huang, J.; Rauscher, S.; Nawrocki, G.; Ran, T.; Feig, M.; de Groot, B. L.; Grubmüller, H.; MacKerell, A. D., Jr. CHARMM36m: an improved force field for folded and intrinsically disordered proteins. *Nat. Methods* **2017**, *14* (1), 71−73.

(6) Maier, J. A.; Martinez, C.; Kasavajhala, K.; Wickstrom, L.; Hauser, K. E.; Simmerling, C. ff14SB: Improving the accuracy of protein side chain and backbone parameters from ff99SB. *J. Chem. Theory Comput.* **2015**, *11* (8), 3696−3713.

(7) Beauchamp, K. A.; Lin, Y. S.; Das, R.; Pande, V. S. Are protein force fields getting better? A systematic benchmark on 524 diverse

NMR measurements. *J. Chem. Theory Comput.* **2012**, *8* (4), 1409−1414.
(8) Li, D. W.; Brüschweiler, R. NMR-based protein potentials. *Angew. Chem., Int. Ed.* **2010**, *49* (38), 6778−6780.
(9) Best, R. B.; Zheng, W.; Mittal, J. Balanced protein-water interactions improve properties of disordered proteins and non-specific protein association. *J. Chem. Theory Comput.* **2014**, *10* (11), 5113−5124.
(10) Wu, H. N.; Jiang, F.; Wu, Y. D. Significantly improved protein folding thermodynamics using a dispersion-corrected water model and a new residue-specific force field. *J. Phys. Chem. Lett.* **2017**, *8* (14), 3199−3205.
(11) Best, R. B.; Mittal, J. Protein simulations with an optimized water model: cooperative helix formation and temperature-induced unfolded state collapse. *J. Phys. Chem. B* **2010**, *114* (46), 14916−14923.
(12) Wang, J.; Cieplak, P.; Kollman, P. A. How well does a restrained electrostatic potential (RESP) model perform in calculating conformational energies of organic and biological molecules? *J. Comput. Chem.* **2000**, *21* (12), 1049−1074.
(13) Jiang, F.; Zhou, C. Y.; Wu, Y. D. Residue-specific force field based on the protein coil library. RSFF1: modification of OPLS-AA/L. *J. Phys. Chem. B* **2014**, *118* (25), 6983−6998.
(14) Jiang, F.; Han, W.; Wu, Y. D. Influence of side chain conformations on local conformational features of amino acids and implication for force field development. *J. Phys. Chem. B* **2010**, *114* (17), 5840−5850.
(15) Best, R. B.; de Sancho, D.; Mittal, J. Residue-specific α-helix propensities from molecular simulation. *Biophys. J.* **2012**, *102* (6), 1462−1467.
(16) Lindorff-Larsen, K.; Piana, S.; Palmo, K.; Maragakis, P.; Klepeis, J. L.; Dror, R. O.; Shaw, D. E. Improved side-chain torsion potentials for the Amber ff99SB protein force field. *Proteins: Struct., Funct., Genet.* **2010**, *78* (8), 1950−1958.
(17) Miller, M. S.; Lay, W. K.; Li, S.; Hacker, W. C.; An, J.; Ren, J.; Elcock, A. H. Reparametrization of protein force field nonbonded interactions guided by osmotic coefficient measurements from molecular dynamics simulations. *J. Chem. Theory Comput.* **2017**, *13* (4), 1812−1826.
(18) Miller, M. S.; Lay, W. K.; Elcock, A. H. Osmotic pressure simulations of amino acids and peptides highlight potential routes to protein force field parameterization. *J. Phys. Chem. B* **2016**, *120* (33), 8217−8229.
(19) Luo, Y.; Roux, B. Simulation of osmotic pressure in concentrated aqueous salt solutions. *J. Phys. Chem. Lett.* **2010**, *1* (1), 183−189.
(20) Ploetz, E. A.; Smith, P. E. A Kirkwood-Buff force field for the aromatic amino acids. *Phys. Chem. Chem. Phys.* **2011**, *13* (40), 18154−18167.
(21) Bentenitis, N.; Cox, N. R.; Smith, P. E. A Kirkwood-Buff derived force field for thiols, sulfides, and disulfides. *J. Phys. Chem. B* **2009**, *113* (36), 12306−12315.
(22) Weerasinghe, S.; Smith, P. E. A Kirkwood-Buff derived force field for methanol and aqueous methanol solutions. *J. Phys. Chem. B* **2005**, *109* (31), 15080−15086.
(23) Pan, A. C.; Jacobson, D.; Yatsenko, K.; Sritharan, D.; Weinreich, T. M.; Shaw, D. E. Atomic-level characterization of protein-protein association. *Proc. Natl. Acad. Sci. U. S. A.* **2019**, *116* (10), 4244−4249.
(24) Hornak, V.; Abel, R.; Okur, A.; Strockbine, B.; Roitberg, A.; Simmerling, C. Comparison of multiple Amber force fields and development of improved protein backbone parameters. *Proteins: Struct., Funct., Genet.* **2006**, *65* (3), 712−725.
(25) Best, R. B.; Hummer, G. Optimized molecular dynamics force fields applied to the helix-coil transition of polypeptides. *J. Phys. Chem. B* **2009**, *113* (26), 9004−9015.
(26) Wang, L. P.; McKiernan, K. A.; Gomes, J.; Beauchamp, K. A.; Head-Gordon, T.; Rice, J. E.; Swope, W. C.; Martínez, T. J.; Pande, V. S. Building a more predictive protein force field: A systematic and reproducible route to AMBER-FB15. *J. Phys. Chem. B* **2017**, *121* (16), 4023−4039.
(27) Doudou, S.; Burton, N. A.; Henchman, R. H. Standard free energy of binding from a one-dimensional potential of mean force. *J. Chem. Theory Comput.* **2009**, *5* (4), 909−918.
(28) Werner, H.-J.; Knowles, P. J.; Knizia, G.; Manby, F. R.; Schütz, M. MOLPRO: A general-purpose quantum chemistry program package. *Wiley Interdiscip. Rev. Comput. Mol. Sci.* **2012**, *2* (2), 242−253.
(29) Kirkwood, J. G.; Buff, F. P. The statistical mechanical theory of solutions. I. *J. Chem. Phys.* **1951**, *19*, 774−777.
(30) Leontyev, I.; Stuchebrukhov, A. Accounting for electronic polarization in non-polarizable force fields. *Phys. Chem. Chem. Phys.* **2011**, *13* (7), 2613−2626.
(31) Joung, I. S.; Cheatham, T. E., III Determination of alkali and halide monovalent ion parameters for use in explicitly solvated biomolecular simulations. *J. Phys. Chem. B* **2008**, *112* (30), 9020−9041.
(32) Lovell, S. C.; Word, J. M.; Richardson, J. S.; Richardson, D. C. The penultimate rotamer library. *Proteins: Struct., Funct., Genet.* **2000**, *40* (3), 389−408.
(33) Zhou, C. Y.; Jiang, F.; Wu, Y. D. Residue-specific force field based on protein coil library. RSFF2: modification of AMBER ff99SB. *J. Phys. Chem. B* **2015**, *119* (3), 1035−1047.
(34) Jiang, F.; Han, W.; Wu, Y.-D. The intrinsic conformational features of amino acids from a protein coil library and their applications in force field development. *Phys. Chem. Chem. Phys.* **2013**, *15*, 3413−3428.
(35) Lifson, S.; Roig, A. On the theory of helix-coil transition in polypeptides. *J. Chem. Phys.* **1961**, *34* (6), 1963−1974.
(36) Moreau, R. J.; Schubert, C. R.; Nasr, K. A.; Török, M.; Miller, J. S.; Kennedy, R. J.; Kemp, D. S. Context-independent, temperature-dependent helical propensities for amino acid residues. *J. Am. Chem. Soc.* **2009**, *131* (36), 13107−13116.
(37) Mao, B.; Tejero, R.; Baker, D.; Montelione, G. T. Protein NMR structures refined with Rosetta have higher accuracy relative to corresponding X-ray crystal structures. *J. Am. Chem. Soc.* **2014**, *136* (5), 1893−1906.
(38) Lindorff-Larsen, K.; Piana, S.; Dror, R. O.; Shaw, D. E. How fast-folding proteins fold. *Science* **2011**, *334* (6055), 517−520.
(39) Sborgi, L.; Verma, A.; Piana, S.; Lindorff-Larsen, K.; Cerminara, M.; Santiveri, C. M.; Shaw, D. E.; de Alba, E.; Muñoz, V. Interaction networks in protein folding via atomic-resolution experiments and long-time-scale molecular dynamics simulations. *J. Am. Chem. Soc.* **2015**, *137* (20), 6506−6516.
(40) Demarest, S. J.; Martinez-Yamout, M.; Chung, J.; Chen, H.; Xu, W.; Dyson, H. J.; Evans, R. M.; Wright, P. E. Mutual synergistic folding in recruitment of CBP/p300 by p160 nuclear receptor coactivators. *Nature* **2002**, *415* (6871), 549−553.
(41) Jensen, M. R.; Houben, K.; Lescop, E.; Blanchard, L.; Ruigrok, R. W.; Blackledge, M. Quantitative conformational analysis of partially folded proteins from residual dipolar couplings: application to the molecular recognition element of Sendai virus nucleoprotein. *J. Am. Chem. Soc.* **2008**, *130* (25), 8055−8061.
(42) Ahmed, M. C.; Papaleo, E.; Lindorff-Larsen, K. How well do force fields capture the strength of salt bridges in proteins? *PeerJ* **2018**, *6*, No. e4967.
(43) Gallagher, T.; Alexander, P.; Bryan, P.; Gilliland, G. L. Two crystal structures of the B1 immunoglobulin-binding domain of streptococcal protein G and comparison with NMR. *Biochemistry* **1994**, *33* (15), 4721−4729.
(44) Tomlinson, J. H.; Ullah, S.; Hansen, P. E.; Williamson, M. P. Characterization of salt bridges to lysines in the protein G B1 domain. *J. Am. Chem. Soc.* **2009**, *131* (13), 4674−4684.
(45) Marinari, E.; Parisi, G. Simulated tempering: A new Monte Carlo scheme. *Europhys. Lett.* **1992**, *19* (6), 451−458.
(46) Jiang, F.; Wu, Y. D. Folding of fourteen small proteins with a residue-specific force field and replica-exchange molecular dynamics. *J. Am. Chem. Soc.* **2014**, *136* (27), 9536−9539.

https://dx.doi.org/10.1021/acs.jctc.9b00251
J. Chem. Theory Comput. 2020, 16, 2494−2507

(47) Piana, S.; Lindorff-Larsen, K.; Shaw, D. E. Protein folding kinetics and thermodynamics from atomistic simulation. *Proc. Natl. Acad. Sci. U. S. A.* **2012**, *109*, 17845−17850.
(48) Piana, S.; Klepeis, J. L.; Shaw, D. E. Assessing the accuracy of physical models used in protein-folding simulations: Quantitative evidence from long molecular dynamics simulations. *Curr. Opin. Struct. Biol.* **2014**, *24*, 98−105.
(49) Schuler, B. Personal communication.
(50) Barua, B.; Lin, J. C.; Williams, V. D.; Kummler, P.; Neidigh, J. W.; Andersen, N. H. The Trp-cage: optimizing the stability of a globular miniprotein. *Protein Eng., Des. Sel.* **2008**, *21* (3), 171−185.
(51) Williams, D. V.; Byrne, A.; Stewart, J.; Andersen, N. H. Optimal salt bridge for Trp-cage stabilization. *Biochemistry* **2011**, *50*, 1143−1152.
(52) Hudaky, P.; Straner, P.; Farkas, V.; Varadi, G.; Toth, G.; Perczel, A. Cooperation between a salt bridge and the hydrophobic core triggers fold stabilization in a Trp-cage miniprotein. *Biochemistry* **2008**, *47* (3), 1007−1016.
(53) Streicher, W. W.; Makhatadze, G. I. Unfolding thermodynamics of Trp-cage, a 20 residue miniprotein, studied by differential scanning calorimetry and circular dichroism spectroscopy. *Biochemistry* **2007**, *46* (10), 2876−2880.
(54) Bunagan, M. R.; Yang, X.; Saven, J. G.; Gai, F. Ultrafast folding of a computationally designed Trp-cage mutant: Trp2-cage. *J. Phys. Chem. B* **2006**, *110* (8), 3759−3763.
(55) Culik, R. M.; Serrano, A. L.; Bunagan, M. R.; Gai, F. Achieving secondary structural resolution in kinetic measurements of protein folding: A case study of the folding mechanism of Trp-cage. *Angew. Chem., Int. Ed.* **2011**, *50* (46), 10884−10887.
(56) Modi, V.; Dunbrack, R. L., Jr. Assessment of refinement of template-based models in CASP11. *Proteins: Struct., Funct., Genet.* **2016**, *84* (Suppl. 1), 260−281.
(57) Hovan, L.; Oleinikovas, V.; Yalinca, H.; Kryshtafovych, A.; Saladino, G.; Gervasio, F. L. Assessment of the model refinement category in CASP12. *Proteins: Struct., Funct., Genet.* **2018**, *86* (Suppl. 1), 152−167.
(58) Heinig, M.; Frishman, D. STRIDE: A web server for secondary structure assignment from known atomic coordinates of proteins. *Nucleic Acids Res.* **2004**, *32*, W500−W502.
(59) Lemkul, J. A.; Huang, J.; Roux, B.; MacKerell, A. D., Jr. An empirical polarizable force field based on the classical Drude oscillator model: Development history and recent applications. *Chem. Rev.* **2016**, *116* (9), 4983−5013.
(60) Duan, L. L.; Feng, G. Q.; Zhang, Q. G. Large-scale molecular dynamics simulation: Effect of polarization on thrombin-ligand binding energy. *Sci. Rep.* **2016**, *6*, 31488.
(61) Ponder, J. W.; Wu, C.; Ren, P.; Pande, V. S.; Chodera, J. D.; Schnieders, M. J.; Haque, I.; Mobley, D. L.; Lambrecht, D. S.; DiStasio, R. A., Jr.; Head-Gordon, M.; Clark, G. N.; Johnson, M. E.; Head-Gordon, T. Current status of the AMOEBA polarizable force field. *J. Phys. Chem. B* **2010**, *114* (8), 2549−2564.
(62) Shi, Y.; Xia, Z.; Zhang, J.; Best, R.; Wu, C.; Ponder, J. W.; Ren, P. The polarizable atomic multipole-based AMOEBA force field for proteins. *J. Chem. Theory Comput.* **2013**, *9* (9), 4046−4063.
(63) Liu, C.; Piquemal, J. P.; Ren, P. AMOEBA+ classical potential for modeling molecular interactions. *J. Chem. Theory Comput.* **2019**, *15* (7), 4122−4139.
(64) Schütz, M.; Hetzer, G.; Werner, H.-J. Low-order scaling local electron correlation methods. I. Linear scaling local MP2. *J. Chem. Phys.* **1999**, *111*, 5691−5705.
(65) Ben-Naim, A. Inversion of Kirkwood-Buff theory of solutions. Application to water−ethanol system. *J. Chem. Phys.* **1977**, *67*, 4884−4890.
(66) Yoo, J.; Aksimentiev, A. Improved parameterization of amine-carboxylate and amine-phosphate interactions for molecular dynamics simulations using the CHARMM and Amber force fields. *J. Chem. Theory Comput.* **2016**, *12* (1), 430−443.
(67) Northrup, S. H.; Hynes, J. T. The stable states picture of chemical reactions. I. Formulation for rate constants and initial condition effects. *J. Chem. Phys.* **1980**, *73* (6), 2700−2714.
(68) Piana, S.; Lindorff-Larsen, K.; Shaw, D. E. How robust are protein folding simulations with respect to force field parameterization? *Biophys. J.* **2011**, *100* (9), L47−L49.
(69) Nerenberg, P. S.; Jo, B.; So, C.; Tripathy, A.; Head-Gordon, T. Optimizing solute-water van der Waals interactions to reproduce solvation free energies. *J. Phys. Chem. B* **2012**, *116* (15), 4524−4534.
(70) Woo, H. J.; Roux, B. Calculation of absolute protein-ligand binding free energy from computer simulations. *Proc. Natl. Acad. Sci. U. S. A.* **2005**, *102* (19), 6825−6830.
(71) Gumbart, J. C.; Roux, B.; Chipot, C. Efficient determination of protein−protein standard binding free energies from first principles. *J. Chem. Theory Comput.* **2013**, *9* (8), 3789−3798.
(72) Bennett, C. H. Efficient estimation of free energy differences from Monte Carlo data. *J. Comput. Phys.* **1976**, *22* (2), 245−268.
(73) MacKerell, A. D.; Bashford, D.; Bellott, M.; Dunbrack, R. L.; Evanseck, J. D.; Field, M. J.; Fischer, S.; Gao, J.; Guo, H.; Ha, S.; Joseph-McCarthy, D.; Kuchnir, L.; Kuczera, K.; Lau, F. T.; Mattos, C.; Michnick, S.; Ngo, T.; Nguyen, D. T.; Prodhom, B.; Reiher, W. E.; Roux, B.; Schlenkrich, M.; Smith, J. C.; Stote, R.; Straub, J.; Watanabe, M.; Wiórkiewicz-Kuczera, J.; Yin, D.; Karplus, M. All-atom empirical potential for molecular modeling and dynamics studies of proteins. *J. Phys. Chem. B* **1998**, *102* (18), 3586−3616.
(74) Bowers, K. J.; Chow, E.; Xu, H.; Dror, R. O.; Eastwood, M. P.; Gregersen, B. A.; Klepeis, J. L.; Kolossváry, I.; Moraes, M. A.; Sacerdoti, F. D.; Salmon, J. K.; Shan, Y.; Shaw, D. E. Scalable algorithms for molecular dynamics simulations on commodity clusters. *Proceedings of the ACM/IEEE Conference on Supercomputing (SC06)*; IEEE: New York, 2006.
(75) Shaw, D. E.; Dror, R. O.; Salmon, J. K.; Grossman, J. P.; Mackenzie, K. M.; Bank, J. A.; Young, C.; Deneroff, M. M.; Batson, B.; Bowers, K. J.; Chow, E.; Eastwood, M. P.; Ierardi, D. J.; Klepeis, J. L.; Kuskin, J. S.; Larson, R. H.; Lindorff-Larsen, K.; Maragakis, P.; Moraes, M. A.; Piana, S.; Shan, Y.; Towles, B. Millisecond-scale molecular dynamics simulations on Anton. *Proceedings of the Conference on High Performance Computing, Networking, Storage and Analysis (SC09)*; ACM: New York, 2009.
(76) Nosé, S. A unified formulation of the constant temperature molecular dynamics methods. *J. Chem. Phys.* **1984**, *81* (1), 511−519.
(77) Hoover, W. G. Canonical dynamics: equilibrium phase-space distributions. *Phys. Rev. A: At., Mol., Opt. Phys.* **1985**, *31* (3), 1695−1697.
(78) Martyna, G. J.; Tobias, D. J.; Klein, M. L. Constant pressure molecular dynamics algorithms. *J. Chem. Phys.* **1994**, *101* (5), 4177−4189.
(79) Tuckerman, M.; Berne, B. J.; Martyna, G. J. Reversible multiple time scale molecular dynamics. *J. Chem. Phys.* **1992**, *97* (3), 1990−2001.
(80) Kräutler, V.; Van Gunsteren, W. F.; Hünenberger, P. H. A fast SHAKE algorithm to solve distance constraint equations for small molecules in molecular dynamics simulations. *J. Comput. Chem.* **2001**, *22* (5), 501−508.
(81) Shan, Y.; Klepeis, J. L.; Eastwood, M. P.; Dror, R. O.; Shaw, D. E. Gaussian split Ewald: a fast Ewald mesh method for molecular simulation. *J. Chem. Phys.* **2005**, *122* (5), 054101.
(82) Sundquist, W. I.; Schubert, H. L.; Kelly, B. N.; Hill, G. C.; Holton, J. M.; Hill, C. P. Ubiquitin recognition by the human TSG101 protein. *Mol. Cell* **2004**, *13* (6), 783−789.
(83) Pornillos, O.; Alam, S. L.; Rich, R. L.; Myszka, D. G.; Davis, D. R.; Sundquist, W. I. Structure and functional interactions of the Tsg101 UEV domain. *EMBO J.* **2002**, *21* (10), 2397−2406.
(84) Ciszak, E.; Smith, G. D. Crystallographic evidence for dual coordination around zinc in the T3R3 human insulin hexamer. *Biochemistry* **1994**, *33* (6), 1512−1517.
(85) Lord, R. S.; Gubensek, F.; Rupley, J. A. Insulin self-association. Spectrum changes and thermodynamics. *Biochemistry* **1973**, *12* (22), 4385−4391.

https://dx.doi.org/10.1021/acs.jctc.9b00251
J. Chem. Theory Comput. 2020, 16, 2494−2507

(86) Peschard, P.; Kozlov, G.; Lin, T.; Mirza, I. A.; Berghuis, A. M.; Lipkowitz, S.; Park, M.; Gehring, K. Structural basis for ubiquitin-mediated dimerization and activation of the ubiquitin protein ligase Cbl-b. *Mol. Cell* **2007**, *27* (3), 474−485.
(87) Huse, M.; Chen, Y. G.; Massagué, J.; Kuriyan, J. Crystal structure of the cytoplasmic domain of the type I TGF beta receptor in complex with FKBP12. *Cell* **1999**, *96* (3), 425−436.
(88) Stanley, W. A.; Filipp, F. V.; Kursula, P.; Schüller, N.; Erdmann, R.; Schliebs, W.; Sattler, M.; Wilmanns, M. Recognition of a functional peroxisome type 1 target by the dynamic import receptor pex5p. *Mol. Cell* **2006**, *24* (5), 653−663.
(89) Friedrich, R.; Fuentes-Prior, P.; Ong, E.; Coombs, G.; Hunter, M.; Oehler, R.; Pierson, D.; Gonzalez, R.; Huber, R.; Bode, W.; Madison, E. L. Catalytic domain structures of MT-SP1/Matriptase, a matrix-degrading transmembrane serine proteinase. *J. Biol. Chem.* **2002**, *277*, 2160−2168.
(90) Read, R. J.; Fujinaga, M.; Sielecki, A. R.; James, M. N. Structure of the complex of Streptomyces griseus protease B and the third domain of the turkey ovomucoid inhibitor at 1.8-Å resolution. *Biochemistry* **1983**, *22* (19), 4420−4433.
(91) Buckle, A. M.; Schreiber, G.; Fersht, A. R. Protein-protein recognition: Crystal structural analysis of a barnase-barstar complex at 2.0-Å resolution. *Biochemistry* **1994**, *33* (30), 8878−8889.
(92) Marquart, M.; Walter, J.; Deisenhofer, J.; Bode, W.; Huber, R. The geometry of the reactive site and of the peptide groups in trypsin, trypsinogen and its complexes with inhibitors. *Acta Crystallogr., Sect. B: Struct. Sci.* **1983**, *39*, 480−490.
(93) Vincent, J. P.; Lazdunski, M. Trypsin-pancreatic trypsin inhibitor association. Dynamics of the interaction and role of disulfide bridges. *Biochemistry* **1972**, *11* (16), 2967−2977.
(94) Ko, T. P.; Liao, C. C.; Ku, W. Y.; Chak, K. F.; Yuan, H. S. The crystal structure of the DNase domain of colicin E7 in complex with its inhibitor Im7 protein. *Structure* **1999**, *7* (1), 91−102.
(95) Keeble, A. H.; Kirkpatrick, N.; Shimizu, S.; Kleanthous, C. Calorimetric dissection of colicin DNase−immunity protein complex specificity. *Biochemistry* **2006**, *45* (10), 3243−3254.
(96) Spiegel, P. C., Jr.; Jacquemin, M.; Saint-Remy, J. M.; Stoddard, B. L.; Pratt, K. P. Structure of a factor VIII C2 domain-immunoglobulin G4kappa Fab complex: Identification of an inhibitory antibody epitope on the surface of factor VIII. *Blood* **2001**, *98* (1), 13−19.
(97) Jacquemin, M. G.; Desqueper, B. G.; Benhida, A.; Vander Elst, L.; Hoylaerts, M. F.; Bakkus, M.; Thielemans, K.; Arnout, J.; Peerlinck, K.; Gilles, J. G.; Vermylen, J.; Saint-Remy, J. M. Mechanism and kinetics of factor VIII inactivation: Study with an IgG4 monoclonal antibody derived from a hemophilia A patient with inhibitor. *Blood* **1998**, *92* (2), 496−506.
(98) Bewley, M. C.; Springer, K.; Zhang, Y. B.; Freimuth, P.; Flanagan, J. M. Structural analysis of the mechanism of adenovirus binding to its human cellular receptor, CAR. *Science* **1999**, *286* (5444), 1579−1583.
(99) Howitt, J.; Bewley, M. C.; Graziano, V.; Flanagan, J. M.; Freimuth, P. Structural basis for variation in adenovirus affinity for the cellular coxsackievirus and adenovirus receptor. *J. Biol. Chem.* **2003**, *278* (28), 26208−26215.
(100) Douangamath, A.; Walker, M.; Beismann-Driemeyer, S.; Vega-Fernandez, M. C.; Sterner, R.; Wilmanns, M. Structural evidence for ammonia tunneling across the ($\beta\alpha$)8 barrel of the imidazole glycerol phosphate synthase bienzyme complex. *Structure* **2002**, *10* (2), 185−193.
(101) Kastritis, P. L.; Bonvin, A. M. Are scoring functions in protein-protein docking ready to predict interactomes? Clues from a novel binding affinity benchmark. *J. Proteome Res.* **2010**, *9* (5), 2216−2225.
(102) Wang, J. H.; Smolyar, A.; Tan, K.; Liu, J. H.; Kim, M.; Sun, Z. Y.; Wagner, G.; Reinherz, E. L. Structure of a heterophilic adhesion complex between the human CD2 and CD58 (LFA-3) counter-receptors. *Cell* **1999**, *97* (6), 791−803.
(103) Zemla, A. LGA: A method for finding 3D similarities in protein structures. *Nucleic Acid Res.* **2003**, *31* (13), 3370−3374.

https://dx.doi.org/10.1021/acs.jctc.9b00251
J. Chem. Theory Comput. 2020, 16, 2494−2507